Equilibrium Chemical Vapor Deposition Growth of Bernal-Stacked Bilayer Graphene

Pei Zhao,*,† Sungjin Kim,‡ Xiao Chen,‡ Erik Einarsson,§ Miao Wang,¶ Yenan Song,† Hongtao Wang,† Shohei Chiashi,† Rong Xiang,‡ and Shigeo Maruyama*,‡

†Institute of Applied Mechanics, Zhejiang University, Zhejiang 310027, China, ‡Department of Mechanical Engineering, The University of Tokyo, Tokyo 113-8656, Japan, §Department of Electrical Engineering, University at Buffalo, New York 14260-2500, United States, and ¶Department of Physics, Zhejiang University, Zhejiang 310027, China

ABSTRACT Using ethanol as the carbon source, self-limiting growth of AB-stacked bilayer graphene (BLG) has been achieved on Cu *via* an equilibrium chemical vapor deposition (CVD) process. We found that during this alcohol catalytic CVD (ACCVD) a source-gas pressure range exists to break the self-limitation of monolayer graphene on Cu, and at a certain equilibrium state it prefers to form uniform BLG with a high surface coverage of ~94% and AB-stacking ratio of nearly 100%. More importantly, once the BLG is completed, this growth shows a self-limiting manner, and an extended ethanol flow time does not result in additional layers. We investigate the mechanism of this equilibrium BLG growth using isotopically labeled ^{13}C-ethanol and selective surface aryl functionalization, and results reveal that during the equilibrium ACCVD process a continuous substitution of graphene flakes occurs to the as-formed graphene and the BLG growth follows a layer-by-layer epitaxy mechanism. These phenomena are significantly in contrast to those observed for previously reported BLG growth using methane as precursor.

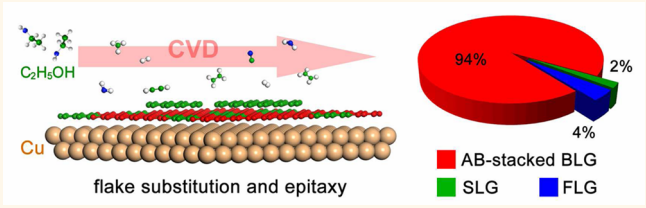

KEYWORDS: chemical vapor deposition · equilibrium · bilayer graphene · layer-by-layer epitaxy · isotope labeling

Graphene, a one-atom-thick crystal of sp^2-bonded carbon, has become one of the most attractive materials for next-generation technologies during the past decade due to its supreme mechanical, electrical, thermal, and other properties.[1−3] To make the many different potential applications of graphene meet their requirements, various production methods for large-scale graphene have been developed, such as epitaxial growth on SiC,[4] Ru,[5] and Pt,[6] reduction of graphene oxide,[7] liquid-phase exfoliation of graphite,[8] and chemical vapor deposition (CVD) of hydrocarbons on transition metals.[9−11] As the most promising route to obtain graphene up to industrial scale, CVD-derived graphene using Cu substrates can exhibit transport properties equivalent to those of exfoliated graphene from mechanical exfoliation.[12,13] It was discussed that during the CVD process, the growth of graphene is restricted to the Cu surface owing to the negligible solubility of carbon in Cu, and more importantly, the absence of Cu catalytic surface after one-layer carbon coverage makes it an ideal substrate for self-limiting growth of monolayer graphene (single-layer graphene, SLG).[14]

However, as a natural zero-bandgap semimetal, there are disadvantages to SLG being fabricated into the core components of modern electronic devices such as field effect transistors, even though graphene has an extremely high electrical carrier mobility.[15] Most of the bandgap-opening trials for graphene are based on surface modifications *via* chemical processes,[16] but they inevitably degrade the carrier mobility in graphene.[15] Bernal-stacked (AB-) bilayer graphene (BLG) can develop a bandgap of up to 250 meV by applying a vertical electric field across the two layers,[17,18] but facile, high-yield synthesis of AB-stacked BLG remains a significant challenge.[19−28] The key point for BLG growth by CVD was to overcome the self-limiting nature of SLG on Cu, in which it is critical to maintain or recover the Cu surface for the effective

* Address correspondence to peizhao@zju.edu.cn, maruyama@photon.t.u-tokyo.ac.jp.

Received for review September 1, 2014 and accepted November 2, 2014.

Published online November 02, 2014
10.1021/nn5049188

catalysis. Hence, compared with the simple self-limiting process of SLG on Cu surface, the growth of BLG has mainly been achieved by complicated pretreatments or designed CVD process, such as spatially arranged Cu substrates,[20,23] percentage-engineered Cu−Ni alloy as catalytic substrates,[21,25] carefully adjusted nucleation pressure of methane,[22,24] a high hydrogen ratio to expose the covered Cu surface,[23] or nonisothermal growth environment with variable temperatures.[28] It is generally believed that during the CVD process the second layer of BLG grows underneath the first-grown layer, as evidenced from isotope-labeling experiments using methane,[26,27] but a layer-by-layer epitaxy mechanism is proposed when spatially arranged Cu substrates are adopted, during which a van der Waals adhesion of the second layer onto the first-grown layer plays the most critical role.[20,23] Besides using methane, graphene growth using ethane or propane as precursor can also exhibit BLG selectivity, but the growth mechanism of the second layer remains unknown.[29] We found this is not the case for the CVD process using ethanol, during which we can achieve layer-by-layer epitaxial growth of equilibrium AB-stacked BLG.

In this work, the self-limiting growth of AB-stacked BLG has been demonstrated *via* equilibrium CVD. Using ethanol as the carbon precursor, it was achieved without involving any specially designed CVD processes or single-crystal or alloy-engineered metal substrates. We found that during this alcohol catalytic CVD (ACCVD) process, a source-gas pressure range exists to break the self-limitation of SLG on Cu, and at a certain equilibrium state it prefers to form uniform BLG with a high surface coverage of ~94% and AB-stacking ratio of nearly 100%. We explain its mechanism using the isotopically labeled ^{13}C-ethanol and selective surface aryl functionalization, and results reveal that during ACCVD a continuous substitution of graphene flakes occurs to the as-formed graphene and the BLG growth follows a layer-by-layer epitaxy mechanism. These phenomena are significantly in contrast to those observed for previously reported BLG growth using methane as precursor.

RESULTS AND DISCUSSION

Ethanol has proven to be an efficient precursor for SLG growth when low-pressure (LP) CVD and folded Cu foil enclosures are adopted.[30] The growth of SLG from ethanol follows a substrate-mediated mechanism in which the Cu surface morphology plays a significant role in the carbon diffusion process and correlated graphene domain formation. A high degree of similarity exists between LPCVD-derived SLG using ethanol and methane as precursors. For example, the surface-mediated growth mechanism and the dendritic graphene domain shapes and, more importantly, the time-independence of SLG growth after the

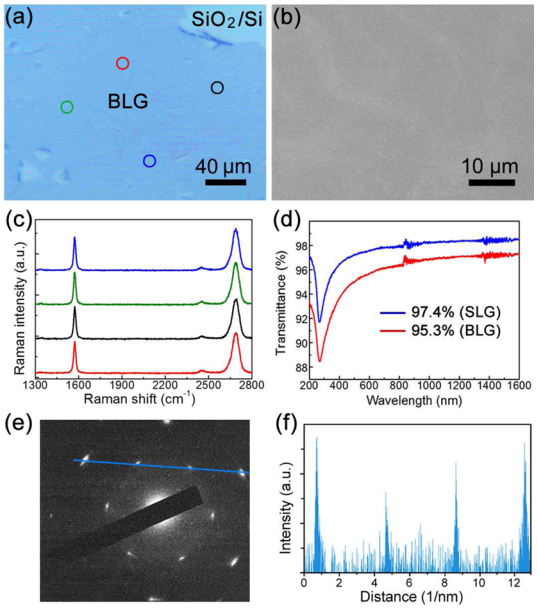

Figure 1. (a) Optical microscope (OM) image of a BLG film on a Si substrate with a 100 nm thick SiO_2 layer. (b) SEM image of as-grown ethanol-derived BLG film on a Cu foil. (c) Typical Raman spectra of BLG measured from four random spots in (a). (d) Transmittance spectra of a transferred BLG film (red), and a reference SLG film (blue). (e) SAED pattern of a bilayer graphene domain, which shows clear 6-fold symmetry. (f) Spot intensities along the blue line in (e).

coverage of one-layer graphene over the Cu surface (the so-called SLG self-limiting process). This is attributed to the absence of a catalytic Cu surface to the stable precursor molecules when the growth of SLG is completed, so that no carbon clusters with dangling bonds for additional graphene layers can be provided.

However, the similarity in graphene growth between ethanol and methane is only valid when the precursor pressure is relatively low. As for methane, it maintains the self-limiting behavior of SLG within a wide range of flow rate or partial pressure. On the other hand, when the ethanol flow rate is increased, a pressure range exists to break the self-limitation of SLG, and additional layers will be formed. This provides the possibility of controllably synthesizing graphene films with the desired layer numbers. This hypothesis is supported by the experimental result that an ethanol partial pressure of 50 Pa and a growth time of 90 min can result in a high coverage of BLG and AB-stacking ratio. At this equilibrium state, ACCVD prefers to form uniform graphene with only two layers. Figure 1a shows a typical optical microscope (OM) image of a BLG film transferred onto a SiO_2/Si substrate. The thickness of the oxide layer on the substrate is 100 nm. In the OM image graphene and substrate both show as bluish color, but the sample uniformity can be evaluated by the slight color contrast. No areas with different colors or contrast are apparent in this sample except for the substrate and sample edges, indicating that the

layer number is uniform across the sample. The scanning electron microscopy (SEM) image of as-grown graphene on Cu shown in Figure 1b also appears to be uniform with no layer contrast, consistent with the observation by optical microscopy. The visible white curves in the SEM image are natural wrinkles of the commercially available Cu foils. The layer number of such ethanol-derived graphene is determined by Raman spectroscopy, and typical Raman spectra collected from circled areas (blue, green, black and red) in Figure 1a are shown in Figure 1c. All these spectra show Raman features of AB-stacked BLG, such as a 2D-band (~2700 cm^{-1}) to G-band (~1582 cm^{-1}) intensity ratio (I_{2D}/I_G) of approximately 1 and an asymmetric 2D-band with a full-width at half-maximum (fwhm) value of 45−60 cm^{-1}. The negligible D-bands at ~1340 cm^{-1} in these spectra are indicative of the very high quality of these ethanol-derived BLG. Due to the optical absorption of exactly 2.3% for one graphene layer,[32] the BLG nature of the graphene film can also be confirmed by UV−vis−NIR spectroscopy. After transfer to a quartz substrate, the graphene film exhibits a transmittance of 95.3% at 550 nm, very close to the theoretical value for BLG (95.4%). The transmittance of a SLG film is also shown in Figure 1d as a reference, which is ~97.4% at 550 nm. Selected-area electron diffraction (SAED) of these ethanol-derived BLG domains using transmission electron microscopy (TEM) shows a single set of 6-fold symmetric diffraction spots (Figure 1e), and the corresponding spot intensities (Figure 1f) along the blue line in the SAED pattern clearly indicate an AB stacking geometry for these graphene samples.

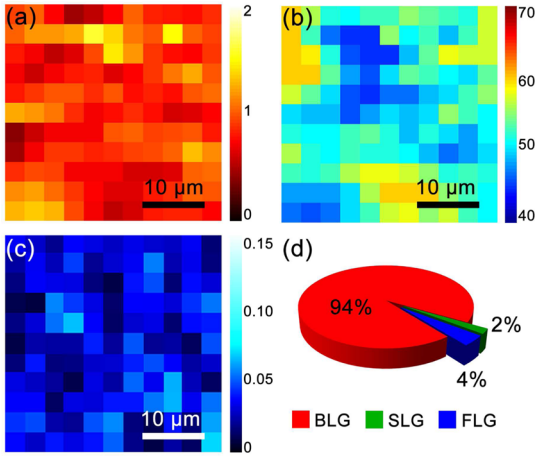

Figure 2. Scanning Raman maps of ethanol-derived BLG for (a) I_{2D}/I_G; (b) fwhm of the 2D-band; (c) I_D/I_G. (d) Corresponding pie chart of graphene coverage for BLG, SLG, and FLG in the ethanol-derived BLG film.

The uniformity and quality of ethanol-derived BLG were further determined by scanning Raman maps of the I_{2D}/I_G, fwhm of 2D-band, and the D-band to G-band intensity ratio (I_D/I_G), as shown in Figure 2a−c. In total, 11 × 11 Raman spectra were collected over a 1000 μm^2 area with ~3 μm spacing resolution. We chose the range of Raman I_{2D}/I_G from 0.7 to 1.3 and the fwhm of the 2D-band from 45 to 60 cm^{-1} to evaluate AB-stacked BLG features, as previously reported.[33] According to the combined results from Figure 2a,b, the ethanol-derived graphene film shows a remarkably high coverage of AB-stacked BLG of ~94%, SLG of ~2% and few-layer graphene (FLG) of ~4%, as shown in Figure 2d. It is noteworthy that twisted BLG with a moiré pattern shows similar Raman features as SLG but a much higher 2D/G ratio and a slight blueshift of the 2D-band.[23,34] Careful investigations of the measured SLG Raman spectra shows no existence of such features from twisted BLG, indicating a 100% AB stacking for the BLG areas.

In order to have a better idea of how the equilibrium BLG grows on Cu surface using ethanol, we interrupted the CVD growth by cutting off the ethanol vapor after different growth periods and present the results in terms of SEM images of as-grown graphene on the Cu surface as shown in Figure 3. When coexisting, BLG areas are displayed in darker color than SLG due to the different secondary electron yields. The brightest contrast is from Cu. After ethanol vapor was flowed for only 5 s, graphene islands were found to have rapidly nucleated and expanded to tens of micrometers and obtained a coverage of over 80% of the Cu surface. The fast formation of graphene within such a short reaction time confirms the efficient conversion of ethanol molecules into graphene. These islands are proven to

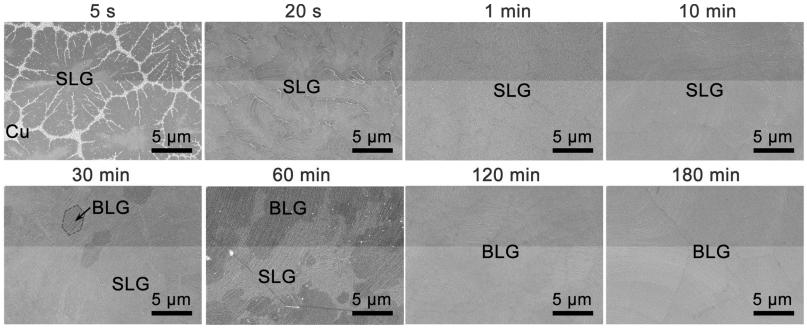

Figure 3. SEM images of as-grown graphene from ethanol on a Cu surface for different growth periods. The flow rate of ethanol was kept at 50 sccm, and the partial pressure of ethanol is ~50 Pa. Two self-limiting processes for SLG and BLG are observed after 1 and 90 min of graphene growth, respectively.

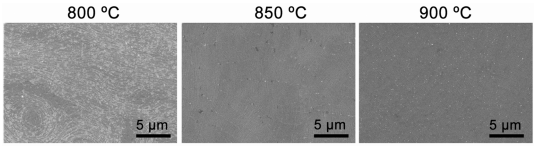

Figure 4. SEM images of as-grown graphene on a Cu surface with an ethanol flow rate of 50 sccm at different growth temperatures. The corresponding pressure is ~50 Pa.

be SLG, as characterized by Raman spectroscopy. Moreover, these SLG islands show dendritic patterns, suggesting a surface-mediated growth process.[30] After 20 s exposure to ethanol, most of the graphene islands have coalesced to form a large sheet, leaving only small unfilled gaps over the surface. Growth of a continuous film of graphene is obtained after 1 min of ethanol flow and maintains the self-limiting behavior of SLG. Prolonged growth periods do not change this self-limiting behavior until after 30 min of ethanol flow, when new graphene islands start to nucleate. These new graphene islands, however, show apparent hexagonal shapes with rigid edges instead of dendritic shapes, indicating a different growth mechanism that is more related with the intrinsic structure of graphene itself. More and more new graphene islands appear with a longer period of ethanol flow and expand or coalesce to form the second layer of graphene. After 90 min, the formation of a continuous second graphene layer completes, and more importantly, the BLG growth achieves an equilibrium state and starts the second self-limiting process but for BLG instead of SLG, as shown by the SEM images of as-grown BLG after 120 and 180 min growth.

The self-limiting growth of BLG shows a high sensitivity on the growth temperature and partial pressure/flow rate of ethanol, due to the significant roles they play in achieving the equilibrium state. The corresponding results are shown in Figure 4 and Figure 5, respectively. When the growth temperature is relatively low, such as 800 °C, after 90 min ethanol flow, the newly nucleated graphene islands cannot efficiently form a continuous second layer. Instead, these islands exhibit as small dots of less than 1 μm size and discretely decorate on the first layer background. An increased growth temperature to 850 °C significantly improved the formation of the second layer, in which most of the new graphene islands have coalesced into a continuous film after 90 min. The self-limiting growth of a complete second layer can be fulfilled with a temperature higher than 900 °C.

A proper partial pressure/flow rate of ethanol is also critical for the equilibrium CVD growth of BLG. As shown in Figure 5, when the partial pressure/flow rate is low, ethanol either forms SLG in a self-limiting manner (10 sccm)[30] or forms a nonuniform graphene film with clearly different layer numbers (30 sccm). On the other hand, when the partial pressure/flow rate is

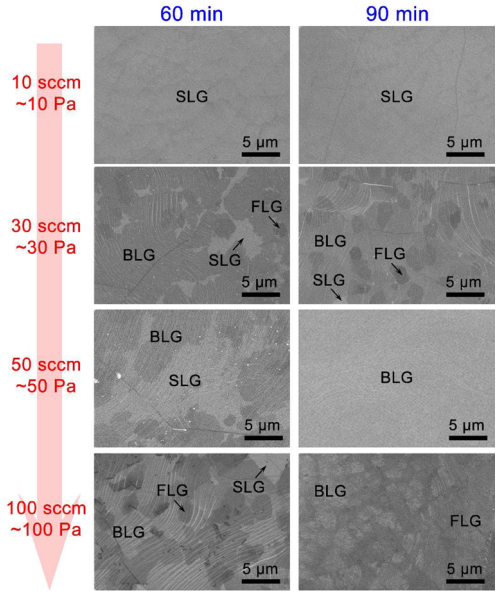

Figure 5. SEM images of ethanol-derived graphene using flow rates of 10, 30, 50, and 100 sccm and growth periods of 60 and 90 min. The partial pressures of ethanol for these flow rates are approximately 10, 30, 50, and 100 Pa, respectively. These recipes show no successful growth of BLG, suggesting the existence of a pressure/flow rate equilibrium to realize the BLG growth.

high, islands of three or more layers easily nucleate when the growth time is less than 60 min and expand to form graphene with different layers after 90 min. These temperature and flow rate dependences suggest the current BLG growth parameters are significant to the equilibrium BLG growth process, not only to initialize the growth of the second layer but also to make it complete and self-limiting.

To further investigate the mechanism for this equilibrium growth of self-limiting BLG using ethanol, we adopted an isotope-labeling method to track the graphene growth route during the CVD process. Due to the expense of $^{13}C_2H_5OH$, its continuous flow for 90 min is not economically sustainable. Our alternative strategy is to grow a uniform SLG by $^{13}C_2H_5OH$ by no-flow ACCVD and demonstrate its equivalence with flow ACCVD and then use $^{12}C_2H_5OH$ to continue the growth for the following 90 min. As shown in Figure S1 (Supporting Information), no-flow ACCVD is efficient to form SLG with high quality, and its dendritic island pattern demonstrates the same surface-mediated process as when flow ACCVD is employed. For BLG growth using isotopic ethanol sources, CVD trials using 3 min of $^{13}C_2H_5OH$ followed by 0, 10, 30, and 70 min of $^{12}C_2H_5OH$ were performed. Because the total growth time is less than 90 min, these samples are not fully covered by BLG areas, and the coexistence of SLG and BLG may help clarify the BLG growth mechanism using ethanol.

We first characterized the areas that are only covered by SLG in these samples, and their corresponding

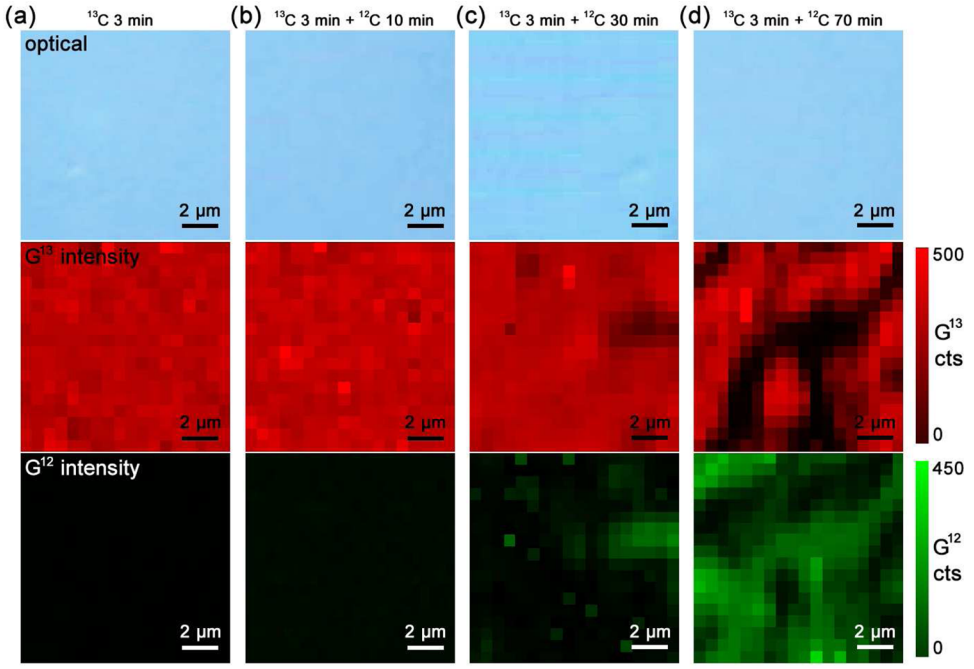

Figure 6. OM images and scanning Raman maps of ^{12}C and ^{13}C G-band peaks for the SLG areas in ethanol-derived graphene samples grown by (a) 3 min $^{13}C_2H_5OH$; (b) 3 min $^{13}C_2H_5OH$ followed by 10 min $^{12}C_2H_5OH$; (c) 3 min $^{13}C_2H_5OH$ followed by 30 min $^{12}C_2H_5OH$; and (d) 3 min $^{13}C_2H_5OH$ followed by 70 min $^{12}C_2H_5OH$. All $^{13}C_2H_5OH$ trials were conducted by no-flow CVD with 0.4 μL of $^{13}C_2H_5OH$, whereas all $^{12}C_2H_5OH$ trials were conducted with flow CVD of 50 sccm $^{12}C_2H_5OH$. Clear substitutions of isotopic graphene flakes are observed in (c) and (d).

OM images and scanning Raman maps of the G-bands for ^{12}C and ^{13}C are shown in Figure 6. Only isotopically pure ^{12}C- or/and ^{13}C-SLG was observed in these samples, evidenced by the Raman G-band peaks located at ~1582 and ~1525 cm^{-1}, respectively. After the formation of SLG by $^{13}C_2H_5OH$ no-flow ACCVD for 3 min, the followed 10 min $^{12}C_2H_5OH$ flow did not change the isotope composition in formed SLG, as shown by the Raman maps of G-band peaks. However, when the $^{12}C_2H_5OH$ flow time was increased to 30 min, some of the ^{13}C areas in formed SLG were substituted by ^{12}C areas, and these ^{13}C-SLG and ^{12}C-SLG areas showed a clear complementary pattern. This pattern is different from the ringlike pattern when sequentially introduced methane is used, in which no such substitution effect has been observed.[26] It needs to be noticed that no G-band peak located at the middle position (~1553 cm^{-1}) was observed in this sample, proving that the ^{12}C and ^{13}C atoms were not well mixed and the substitution of ^{13}C by ^{12}C occurred only in a flake-by-flake manner. When the $^{12}C_2H_5OH$ flow time was further increased to 70 min, the isotope substitution became more severe, and more than half of the ^{13}C areas in initially formed SLG were substituted by ^{12}C areas, with the clear flake-by-flake manner.

Of more importance is the formation of AB-stacked BLG. Figure 7 shows the Raman analysis of a graphene sample with coexisting SLG and BLG, as well as both ^{12}C and ^{13}C areas. This was grown from 3 min of $^{13}C_2H_5OH$ no-flow ACCVD followed by 70 min of

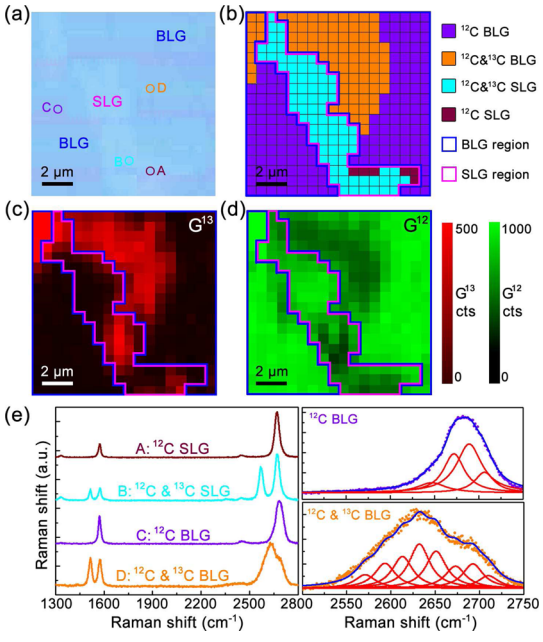

Figure 7. Raman analysis of a graphene sample with coexistence of both SLG and BLG and ^{12}C and ^{13}C areas. (a) OM image of the measured sample, in which SLG and BLG areas are clearly visible by their different color contrast. (b) Graphene flakes with different layer numbers and isotope compositions. (c, d) Scanning Raman maps of ^{12}C and ^{13}C G-band peaks in the sample, respectively. (e) Typical Raman spectra measured from circled spots in (a) and the decomposed 2D-band peaks for ^{12}C BLG and ^{12}C and ^{13}C BLG.

$^{12}C_2H_5OH$ flow ACCVD. The OM image of measured area on this sample is shown in Figure 7a, in which the

SLG and BLG areas are clearly visible by their different color contrast. Scanning Raman results show that the SLG and BLG areas are formed by only ^{12}C atoms or both ^{12}C and ^{13}C atoms, but not by only ^{13}C atoms. Graphene flakes with different layer numbers or isotope compositions are indicated by different colors in Figure 7b, and the SLG and BLG areas are circled by pink and blue lines, respectively. Most (~93%) of the SLG area is composed of both ^{12}C and ^{13}C atoms, due to the isotope substitution from sequentially introduced $^{12}C_2H_5OH$, as previously mentioned. On the other hand, for the BLG area in this sample, only ~35% is composed of both isotopes, whereas the rest is formed by only ^{12}C atoms. The G-band Raman maps of ^{13}C and ^{12}C graphene flakes are shown in parts c and d of Figure 7, respectively, but these G-band patterns for ^{13}C and ^{12}C graphene are not consistent with the SLG and BLG distributions. This inconsistency shows that the isotope substitution has no dependence on the graphene layer numbers. Typical Raman spectra of ^{12}C SLG, ^{12}C and ^{13}C SLG, ^{12}C BLG, and ^{12}C and ^{13}C BLG are shown in the left panel of Figure 7e, measured from the areas circled by brown, cyan, violet, and orange in Figure 7a, respectively. For ^{12}C and ^{13}C SLG, the Raman spectrum consists of both ^{12}C and ^{13}C G-band peaks, and both the I_{2D}/I_G for ^{12}C and ^{13}C peaks are larger than 3. We characterized this Raman spectrum as from ^{12}C and ^{13}C SLG other than from a twist ^{12}C and ^{13}C BLG is due to the fact that no frequency shift is observed for the two 2D-band peaks, as well as the slightly brighter color for SLG in the OM image. The right panels of Figure 7e show the decomposed Raman spectra for ^{12}C BLG and AB-stacked ^{12}C and ^{13}C BLG. The spectra of ^{12}C BLG and ^{12}C and ^{13}C BLG are fitted by four and eight symmetric Lorentzian shapes, respectively, representing their four and eight allowed transitions. The decomposition of the 2D-band Raman peak in ^{12}C and ^{13}C BLG into eight peaks also demonstrates a modified electronic dispersion but is still consistent with the double-resonance Raman theory for the 2D-band in AB-stacked BLG.

A most important issue in the growth mechanism study of equilibrium BLG is the growth sequence of the two layers. It is generally believed that when methane is used as precursor the second graphene layer is grown underneath the first one[26,27] at the same nucleation spots but slower growth rates. However, some reports also proposed that the second graphene layer can form above the first one, as long as carbon fragments catalyzed from elsewhere are brought above the first layer and adhere by van der Waals interaction.[20,23] To characterize the growth sequence of the two layers in ethanol-derived BLG, we employed aryl group functionalization on isotopically labeled BLG samples to create sp^3-type defects on the top surface of graphene using 4-nitrophenyldiazonium tetrafluoroborate ($NO_2-C_6H_4N_2^+BF_4^-$)[35] and detect the corresponding changes in the Raman spectra from different

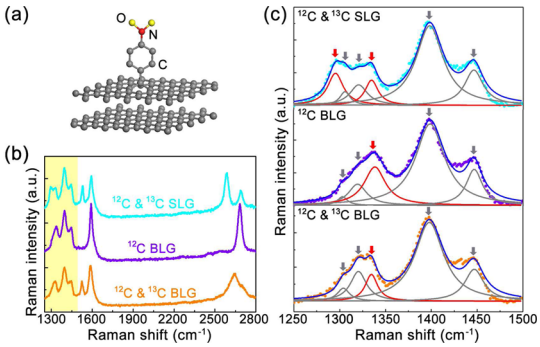

Figure 8. (a) Schematic of aryl group functionalization to BLG, which only modifies the top layer of a BLG film. (b) Typical Raman spectra of a modified isotopically labeled graphene sample, measured from ^{12}C and ^{13}C SLG, ^{12}C BLG, and ^{12}C and ^{13}C BLG areas. (c) Enlarged D-band spectra from the highlighted areas in (b). Red and gray arrows indicate the newly generated defect peaks in graphene and peaks from aryl groups, respectively.

modified SLG and BLG areas. When BLG is transferred onto a Si/SiO_2 substrate, the $NO_2-C_6H_4N_2^+BF_4^-$ molecules selectively modify the top layer and leave the bottom layer unchanged. A schematic of aryl-group functionalization for BLG is shown in Figure 8a, and the Raman spectra of different modified areas are shown in Figure 8b. The D-band peaks highlighted by yellow in Figure 8b are enlarged in Figure 8c, and red and gray arrows indicate the newly generated defect peaks in graphene and peaks from aryl groups, respectively.[36] After aryl-group functionalization for ^{12}C and ^{13}C SLG, two apparent D-band peaks (indicated by red arrows) were detected at ~1290 and 1340 cm^{-1}, corresponding to the defect peaks in ^{13}C and ^{12}C graphene, respectively. The assignment of the 1290 cm^{-1} peak to the D-band peak of ^{13}C graphene is based on the aryl-group functionalization results of isotopically pure ^{13}C graphene. The coexistence of these two D-band peaks shows that both ^{12}C and ^{13}C graphene flakes are modified, which also confirms the one-layer nature of this graphene area. However, for modified ^{12}C and ^{13}C BLG, only one D-band peak located at ~1340 cm^{-1} was observed, which was from the defect sites in ^{12}C graphene flakes. Because the second layer in the isotopically labeled BLG is formed entirely from $^{12}C_2H_5OH$, considering that aryl groups only modify the top layers, these surface functionalization experiments clearly demonstrate that the new graphene layer is grown on top of the previous one when ethanol is used as the precursor. This result is consistent with the previously shown SEM images with newly grown second layers, which have graphene-related hexagonal shapes instead of Cu-related dendritic shapes.

Based on the evidence shown above, we propose the mechanism of equilibrium BLG growth from ethanol as a layer-by-layer epitaxy. As shown in Figure 9, with a proper partial pressure of ethanol, after the formation of SLG from a surface-mediated process, the graphene growth first

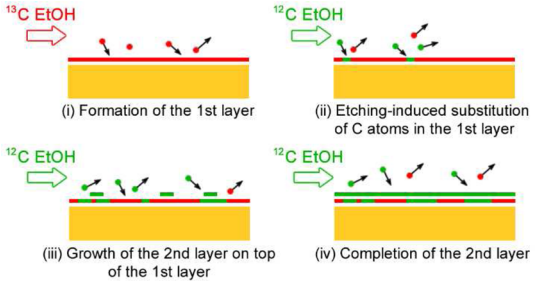

Figure 9. Schematic the layer-by-layer epitaxy mechanism for equilibrium BLG growth using ethanol as CVD precursor.

maintains the self-limiting manner for a certain period but with flake substitution triggered by newly introduced ethanol. We attribute the origin of this substitution to the etching effect of some decomposed products from ethanol, such as H_2, H_2O, *etc.* With longer growth time and a proper kinetic equilibrium, carbon fragments formed by decomposed ethanol products start to nucleate on top of the first graphene layer by the van de Waals interaction and then expand and coalesce into a continuous layer with a lower growth rate than the first layer. Moreover, during the growth of the second graphene layer, flake substitution occurs in both layers.

CONCLUSIONS

We demonstrate the first self-limiting growth of AB-stacked BLG films on Cu using an equilibrium ACCVD process without any other specially designed growth process, single-crystal, or alloy-engineered metal substrates. During the graphene growth at the equilibrium state, two self-limitations occur at different growth stages for SLG and BLG, respectively. SLG is formed first with a surface-mediated mechanism, followed by its self-limiting period for ~30 min. Hexagonal-shaped graphene grains of the second layer appear later and expand into a continuous sheet with a slower rate, and the growth of this BLG film maintains the self-limiting manner for no shorter than 90 min. The equilibrium BLG has a high surface coverage of ~94% and an AB-stacking ratio of ~100%. Isotope-labeling experiments using $^{12}C_2H_5OH$, $^{13}C_2H_5OH$, and selective surface aryl functionalization on the top layer of grown ^{12}C and ^{13}C BLG prove that this self-limiting growth of BLG using ethanol occurs with a layer-by-layer epitaxy mechanism with continuous flake substitution in formed layers. This is different from the growth mechanism of BLG using methane as carbon precursor, in which no substitution occurs and the new layer grows underneath the formed layer. Although only the equilibrium growth of self-limiting AB-stacked BLG is presented here, we believe that such growth can be extended to uniform graphene with more layers, hence help understand more thermal dynamic processes for graphene growth and advance the ongoing efforts toward controlled and inexpensive approaches for scalable graphene production.

METHODS

Graphene Synthesis. An ACCVD process was used for the self-limiting BLG growth, as described elsewhere.[30] In brief, after surface cleaning the commercially available Cu foil (10 μm thick, Nippon Denkai Co., Ltd.) was folded into an enclosure with the remaining three sides carefully crimped and loaded into a hot-wall CVD quartz chamber (26 mm, i.d.). The enclosure was annealed at 1000 °C for 20 min before 50 sccm ethanol vapor was introduced. The partial pressure of ethanol was kept at approximately 50 Pa. The growth lasted for different periods of several seconds to 180 min. For BLG growth from isotopic ethanol sources, an equivalent no-flow CVD process was adopted.[31] In this case, 0.4 μL of $^{13}C_2H_5OH$ (99%, Cambridge Isotope Laboratories, Inc.) was first introduced for 3 min to finish the growth of the first layer, followed by evacuating the ^{13}C residues and introducing 50 sccm of $^{12}C_2H_5OH$ for the desired growth time.

Graphene Transfer. For graphene transfer, the inside surface of the unfolded Cu foil enclosure was spin-coated with a thin layer of poly(methyl methacrylate) (PMMA) and baked at 150 °C, and the outside surface was treated with O_2 plasma to remove the unnecessary graphene and graphite layers. The supported Cu foil was then etched by a 1 M $FeCl_3$ solution to isolate the graphene/PMMA film for its transfer to arbitrary substrates. Finally, the PMMA layer was removed by a hot acetone bath. If the BLG was transferred to SiO_2/Si substrate for surface functionalization, it needs an additional annealing process at 360 °C for 3 h with a 100 sccm hydrogen flow to increase the interface adhesion between graphene and the substrate.

Surface Functionalization. The selective surface functionalization of the BLG top layer was conducted using a mixed aqueous solution of 30 mL 20 mM 4-nitrobenzenediazonium tetrafluoroborate and 6 mL of 1% w/v sodium dodecyl sulfate. Annealed BLG/SiO_2/Si sample was immersed in the solution, gently stirred for 5 h at 35 °C, and then placed in DI water overnight to remove the salt residues. Finally, the sample was repeatedly rinsed by DI water and dried by nitrogen flow.

Characterization. Characterization of as-grown and transferred graphene samples was carried out by scanning electron microscopy (SEM, 5 kV, S-4800, Hitachi Co., Ltd.), transmission electron microscopy (TEM, 80 kV, JEM-2100, JEOL Co., Ltd.), UV−vis−NIR spectroscopy (UV-3600, Shimadzu Co., Ltd.), and micro-Raman spectroscopy (Renishaw inVia system, Renishaw plc).

Conflict of Interest: The authors declare no competing financial interest.

Supporting Information Available: Supporting figures. This material is available free of charge *via* the Internet at http://pubs.acs.org.

Acknowledgment. Part of this work was financially supported by JSPS Grants-in-Aid for Scientific Research (22226006, 23760180, 23760179, 25630063, 25107002, 25220602), JST-EC DG RTD Coordinated Research Project "IRENA" within the Strategic International Collaborative Research Program (SICORP), Takuetsu Program "GMSI" by the Ministry of Education, Culture, Sport, Science and Technology of Japan, Zhejiang Provincial Natural Science Foundation of China (Z1110057), the Fundamental Research Funds for the Central Universities of China (2014QNA4033), the National Natural Science Foundation of China (61471317), and the National Key Scientific Instruments and Equipment Development Project of China. We also acknowledge Mr. Ke Cao from the School of Materials Science and Engineering at Zhejiang University for the TEM measurements.

REFERENCES AND NOTES

1. Novoselov, K. S.; Falko, V. I.; Colombo, L.; Gellert, P. R.; Schwab, M. G.; Kim, K. A Roadmap for Graphene. *Nature* **2012**, *490*, 192–200.
2. Lee, C.; Wei, X.; Kysar, J. W.; Hone, J. Measurement of the Elastic Properties and Intrinsic Strength of Monolayer Graphene. *Science* **2008**, *321*, 385–388.
3. Baringhaus, J.; Ruan, M.; Edler, F.; Tejeda, A.; Sicot, M.; Taleb, I.; Li, A.-P.; Jiang, Z.; Conrad, E. H.; Berger, C.; *et al.* Exceptional Ballistic Transport in Epitaxial Graphene Nanoribbons. *Nature* **2014**, *506*, 349–354.
4. Berger, C.; Song, Z.; Li, X.; Wu, X.; Brown, N.; Naud, C.; Mayou, D.; Li, T.; Hass, J.; Marchenkov, A. N.; *et al.* Electronic Confinement and Coherence in Patterned Epitaxial Graphene. *Science* **2006**, *312*, 1191–1196.
5. Sutter, P. W.; Flege, J.-I.; Sutter, E. A. Epitaxial Graphene on Ruthenium. *Nat. Mater.* **2008**, *7*, 406–411.
6. Gao, L.; Ren, W.; Xu, H.; Jin, L.; Wang, Z.; Ma, T.; Ma, L.-P.; Zhang, Z.; Fu, Q.; Peng, L.-M.; *et al.* Repeated Growth and Bubbling Transfer of Graphene With Millimetre-Size Single-Crystal Grains Using Platinum. *Nat. Commun.* **2012**, *3*, 699.
7. Stankovich, S.; Dikin, D. A.; Piner, R. D.; Kohlhaas, K. A.; Kleinhammes, A.; Jia, Y.; Wu, Y.; Nguyen, S. T.; Ruoff, R. S. Synthesis of Graphene-Based Nanosheets *via* Chemical Reduction of Exfoliated Graphite Oxide. *Carbon* **2007**, *45*, 1558–1565.
8. Hernandez, Y.; Nicolosi, V.; Lotya, M.; Blighe, F. M.; Sun, Z.; De, S.; McGovern, I. T.; Holland, B.; Byrne, M.; Gun'Ko, Y. K.; *et al.* High-Yield Production of Graphene by Liquid-Phase Exfoliation of Graphite. *Nat. Nanotachnol.* **2008**, *3*, 563–568.
9. Reina, A.; Jia, X. T.; Ho, J.; Nezich, D.; Son, H. B.; Bulovic, V.; Dresselhaus, M. S.; Kong, J. Large Area, Few-Layer Graphene Films on Arbitrary Substrates by Chemical Vapor Deposition. *Nano Lett.* **2009**, *9*, 30–35.
10. Kim, K. S.; Zhao, Y.; Jang, H.; Lee, S. Y.; Kim, J. M.; Kim, K. S.; Ahn, J.-H.; Kim, P.; Choi, J.-Y.; Hong, B. H. Large-Scale Pattern Growth of Graphene Films for Stretchable Transparent Electrodes. *Nature* **2009**, *457*, 706–710.
11. Li, X.; Cai, W.; An, J.; Kim, S.; Nah, J.; Yang, D.; Piner, R.; Velamakanni, A.; Jung, I.; Tutuc, E.; *et al.* Large-Area Synthesis of High-Quality and Uniform Graphene Films on Copper Foils. *Science* **2009**, *324*, 1312–1314.
12. Bae, S.; Kim, H.; Lee, Y.; Xu, X.; Park, J.-S.; Zheng, Y.; Balakrishnan, J.; Lei, T.; Kim, H. R.; Song, Y. I.; *et al.* Roll-to-Roll Production of 30-in. Graphene Films for Transparent Electrodes. *Nat. Nanotechnol.* **2010**, *5*, 574–578.
13. Petrone, N.; Dean, C. R.; Meric, I.; van der Zande, A. M.; Huang, P. Y.; Wang, L.; Muller, D.; Shepard, K. L.; Hone, J. Chemical Vapor Deposition-Derived Graphene with Electrical Performance of Exfoliated Graphene. *Nano Lett.* **2012**, *12*, 2751–2756.
14. Li, X.; Cai, W.; Colombo, L.; Ruoff, R. S. Evolution of Graphene Growth on Ni and Cu by Carbon Isotope Labeling. *Nano Lett.* **2009**, *9*, 4268–4272.
15. Schwierz, F. Graphene Transistors. *Nat. Nanotechnol.* **2010**, *5*, 487–496.
16. Elias, D. C.; Nair, R. R.; Mohiuddin, T. M. G.; Morozov, S. V.; Blake, P.; Halsall, M. P.; Ferrari, A. C.; Boukhvalov, D. W.; Katsnelson, M. I.; Geim, A. K.; *et al.* Control of Graphene's Properties by Reversible Hydrogenation: Evidence for Graphane. *Science* **2009**, *323*, 610–613.
17. Zhang, Y.; Tang, T.-T.; Girit, C.; Hao, Z.; Martin, M. C.; Zettl, A.; Crommie, M. F.; Shen, Y. R.; Wang, F. Direct Observation of a Widely Tunable Bandgap in Bilayer Graphene. *Nature* **2009**, *459*, 820–823.
18. Mak, K. F.; Lui, C. H.; Shan, J.; Heinz, T. F. Observation of an Electric-Field-Induced Band Gap in Bilayer Graphene by Infrared Spectroscopy. *Phys. Rev. Lett.* **2009**, *102*, 256405.
19. Lee, S.; Lee, K.; Zhong, Z. Wafer Scale Homogeneous Bilayer Graphene Films by Chemical Vapor Deposition. *Nano Lett.* **2010**, *10*, 4702–4707.
20. Yan, K.; Peng, H.; Zhou, Y.; Li, H.; Liu, Z. Formation of Bilayer Bernal Graphene: Layer-by-Layer Epitaxy *via* Chemical Vapor Deposition. *Nano Lett.* **2011**, *11*, 1106–1110.
21. Liu, X.; Fu, L.; Liu, N.; Gao, T.; Zhang, Y. F.; Liao, L.; Liu, Z. F. Segregation Growth of Graphene on Cu-Ni Alloy for Precise Layer Control. *J. Phys. Chem. C* **2011**, *115*, 11976–11982.
22. Sun, Z.; Raji, A.-R. O.; Zhu, Y.; Xiang, C.; Yan, Z.; Kittrell, C.; Samuel, E. L. G.; Tour, J. M. Large-Area Bernal-Stacked Bi-, Tri-, and Tetralayer Graphene. *ACS Nano* **2012**, *6*, 9790–9796.
23. Liu, L.; Zhou, H.; Cheng, R.; Yu, W. J.; Liu, Y.; Chen, Y.; Shaw, J.; Zhong, X.; Huang, Y.; Duan, X. High-Yield Chemical Vapor Deposition Growth of High-Quality Large-Area AB-Stacked Bilayer Graphene. *ACS Nano* **2012**, *6*, 8241–8249.
24. Zhou, H.; Yu, W. J.; Liu, L.; Cheng, R.; Chen, Y.; Huang, X.; Liu, Y.; Wang, Y.; Huang, Y.; Duan, X. Chemical Vapour Deposition Growth of Large Single Crystals of Monolayer and Bilayer Graphene. *Nat. Commun.* **2013**, *4*, 2096.
25. Liu, W.; Kraemer, S.; Sarkar, D.; Li, H.; Ajayan, P. M.; Banerjee, K. Controllable and Rapid Synthesis of High-Quality and Large-Area Bernal Stacked Bilayer Graphene Using Chemical Vapor Deposition. *Chem. Mater.* **2013**, *26*, 907–915.
26. Li, Q.; Chou, H.; Zhong, J.-H.; Liu, J.-Y.; Dolocan, A.; Zhang, J.; Zhou, Y.; Ruoff, R. S.; Chen, S.; Cai, W. Growth of Adlayer Graphene on Cu Studied by Carbon Isotope Labeling. *Nano Lett.* **2013**, *13*, 486–490.
27. Fang, W.; Hsu, A. L.; Caudillo, R.; Song, Y.; Birdwell, A. G.; Zakar, E.; Kalbac, M.; Dubey, M.; Palacios, T.; Dresselhaus, M. S.; *et al.* Rapid Identification of Stacking Orientation in Isotopically Labeled Chemical-Vapor Grown Bilayer Graphene by Raman Spectroscopy. *Nano Lett.* **2013**, *13*, 1541–1548.
28. Sun, H.-B.; Wu, J.; Han, Y.; Wang, J.-Y.; Song, F.-Q.; Wan, J.-G. Nonisothermal Synthesis of AB-Stacked Bilayer Graphene on Cu Foils by Atmospheric Pressure Chemical Vapor Deposition. *J. Phys. Chem. C* **2014**, *118*, 14655–14661.
29. Wassei, J. K.; Mecklenburg, M.; Torres, J. A.; Fowler, J. D.; Regan, B. C.; Kaner, R. B.; Weiller, B. H. Chemical Vapor Deposition of Graphene on Copper from Methane, Ethane and Propane: Evidence for Bilayer Selectivity. *Small* **2012**, *8*, 1415–1422.
30. Zhao, P.; Kumamoto, A.; Kim, S.; Chen, X.; Hou, B.; Chiashi, S.; Einarsson, E.; Ikuhara, Y.; Maruyama, S. Self-Limiting Chemical Vapor Deposition Growth of Monolayer Graphene from Ethanol. *J. Phys. Chem. C* **2013**, *117*, 10755–10763.
31. Xiang, R.; Hou, B.; Einarsson, E.; Zhao, P.; Harish, S.; Morimoto, K.; Miyauchi, Y.; Chiashi, S.; Tang, Z.; Maruyama, S. Carbon Atoms in Ethanol Do Not Contribute Equally to Formation of Single-Walled Carbon Nanotubes. *ACS Nano* **2013**, *7*, 3095–3103.
32. Nair, R. R.; Blake, P.; Grigorenko, A. N.; Novoselov, K. S.; Booth, T. J.; Stauber, T.; Peres, N. M. R.; Geim, A. K. Fine Structure Constant Defines Visual Transparency of Graphene. *Science* **2008**, *320*, 1308.
33. Peng, Z.; Yan, Z.; Sun, Z.; Tour, J. M. Direct Growth of Bilayer Graphene on SiO2 Substrates by Carbon Diffusion through Nickel. *ACS Nano* **2011**, *5*, 8241–8247.
34. Ni, Z.; Wang, Y.; Yu, T.; You, Y.; Shen, Z. Reduction of Fermi velocity in folded graphene observed by resonance Raman spectroscopy. *Phys. Rev. B* **2008**, *77*, 235403.
35. Bekyarova, E.; Itkis, M. E.; Ramesh, P.; Berger, C.; Sprinkle, M.; de Heer, W. A.; Haddon, R. C. Chemical Modification of Epitaxial Graphene: Spontaneous Grafting of Aryl Groups. *J. Am. Chem. Soc.* **2009**, *131*, 1336–1337.
36. Liu, Y.-C.; McCreery, R. L. Reactions of Organic Monolayers on Carbon Surfaces Observed with Unenhanced Raman Spectroscopy. *J. Am. Chem. Soc.* **1995**, *117*, 11254–11259.